Numerical Modeling of Cross-Fed Orifice Flows for Shear-Thinning Fluids

Changjin Yoon⋆, Stephen D. Heister⋆, Guoping Xia⋆ and Charles L. Merkle⋆
⋆Purdue University, West Lafyaette, IN, USA
Maurice J. Zucrow Laboratories, 500 Allison Rd, West Lafayette, IN 47907, USA

Abstract

Full Navier-Stokes simulations are presented in order to reveal the unsteady structure of the cross-fed orifice flows for shear-thinning fluids. Comparing with straightly-fed shear-thinning and cross-fed Newtonian fluid simulations, it is found that the cross-fed orifice flows for shear-thinning fluids have larger and more distinct vortex structure generated by the horseshoe vortex. Furthermore, the effects of orifice Length-to-Diameter (L/D), Reynolds number, and cross velocity in a manifold on the discharge coefficients are studied and summarized. In particular, as the cross velocity in a manifold increases, it is found that the discharge coefficients are significantly reduced because of strong asymmetric flow resistance caused by a shear-thinning behavior.

1. Introduction

There is an interest in gelling propellants in order to improve safety, reduced volatility and minimized leakage from spills, and to potentially permit the addition of energetic powders to liquid propellants. Most formulations of interest exhibit a shear-thinning behavior wherein fluid viscosity decreases with increasing shear rate. Typical gels are unlikely to flow when no forces are exerted because of this shear-thinning behaviour. However, non-Newtonian shear-thinning gels have been much less studied than their Newtonian counterparts and all flow processes including internal flow, atomization and combustion are quite poorly understood. All these processes are known to be considerably influenced by the rheology of gels and, in particular, for propellant feeding or injection operation, the rheological behaviour is expected to cause the unique flow structure and exit flow influencing the subsequent processes such as the atomization and burning as an initial condition. It is this issue that is the central focus of the present study.

Plain-orifice atomizers have been mostly used as an element of injection system in prior gel propulsion studies due to ease of fabrication and overall performance. Previous successful prototypes demonstrated the usefulness and excellence of the plain-orifice atomizer as an element of pintle [1] and impinging jet injectors [2, 3] in their firing tests of practical systems. Sometimes, a contracting flowpath [4, 5] has been used in lab-scale experiments as a means to provide more continual acceleration of the fluid within the injection passage. Early studies on orifice flows focused on the steady discharge characteristics [6] of Newtonian fluids, but the interests are moving to the unsteady phenomena that occur inside an orifice passage. Several factors are known to serve as instability sources that can lead the unsteadiness. Cavitation is one of primary instability sources and occurs when the local pressure near the inlet lip is lower than the vapour pressure due to strong accelerations by the sudden contraction. Even under the non-cavitating condition, the recirculating vortex is still located at the inlet lip and oscillates with a separation to satellite vortices as illustrated in Fig. 1a. [7, 8] This unstable behaviour of the vena contracta also generates the mass pulsations at the orifice exit as cavitation. Pulsations of about 1-2 % are attributed to non-cavitating laminar hydrodynamic instabilities of the vena contracta near the inlet lip from Canino and Heister's simulations [7] of axially-fed (axisymmetric) passages in Figure 1(a). Furthermore, the axisymmetric calculations by Yoon and Heister [9] exhibit the potential occurrence of the unsteadiness for shear-thinning orifice flows.

The extreme three-dimensionality imposed by the presence of a cross-flow within the injector manifold has been much less studied in both experimental and computational/analytical literature despite the presence of such flows in virtually all multi-element injectors. The cross-flow in a manifold typically causes the asymmetric flow structure inside an orifice passage as Figure 1(b). The size of a recirculation zone on the windward side is significantly expanded

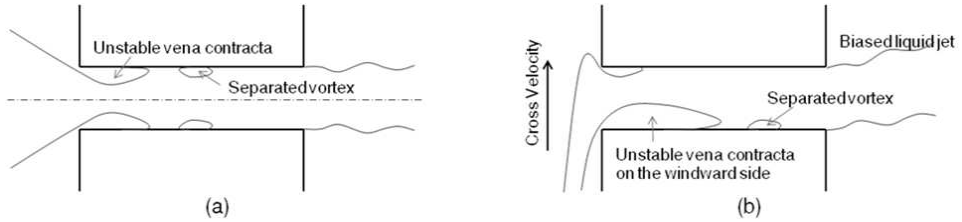

Figure 1: Unsteadiness in Newtonian orifice flows: (a) Axially-fed type (b) Cross-fed type

when compared with the one on the leeward side. This unbalanced size of the vena contractas may influence the unsteadiness due to the hydrodynamic instabilities. Considering the fact that cavitation significantly affects the liquid jet deformation confirmed by the recent experiments, spatially biased instabilities induced by a cross velocity may lead to a biased velocity profile at the orifice exit, subsequently to a unique spray development.

There have been a few relevent experimental studies of the flowfield in question for the case of Newtonian fluids. Strakey and Talley [10] studied the effect of cross flow and orifice length-to-diameter ratio on the discharge coefficient and cavitational characteristics for the impinging jet injector applications. They developed the analytical model based on quasi-one dimensional fluid dynamics in order to estimate the discharge coefficient. The model showed a good agreement in discharge coefficient and the onset of cavitation with measured data except for short orifice passages, L/D < 3. As a result of experiments, the discharge coefficient was found to decrease as cross velocity increased and orifice L/D ratio increased and these trends qualitatively matches well with an analytical model. Nurick et al. [11, 12] investigated the effect of turning angle and orifice length-to-diameter ratio on the discharge coefficient.

Bunnell [13] performed a computational study of cross-fed Newtonian orifice flows for both cavitating and non-cavitating conditions. His results indicated that the vortical structure at the orifice exit is likely to move in transverse direction and this behaviour is more violent under non-cavitating condition than for cavitating conditions. For the non-cavitating flow, a great amount of structure is revealed by the vorticity transport from the cross-flow in a manifold and this structure is also found in experimental observation.

To the authors knowledge, this problem has not been studied computationally for shear thinning fluids. The objective of the current study is to characterize mean and transient characteristics of cross-fed orifice flows for shear-thinning fluids. The flow characterization using the introduction of the discharge coefficient will help us to estimate the orifice exit flow, and to deliver the information for the jet and spray analyses. The effect of the manifold/injection velocity ratio and orifice length-to-diameter ratio is considered. Furthermore, the shear-thinning cross flow will be compared and discussed with the Newtonian one. Section 2 provides a description of the computational model while Sections 3 and 4 provide illumination of the unsteady flowfield and results of the parametric studies, respectively. Conclusions of the work are provided in Section 5.

2. Numerical Model Description

2.1 Solution Methods

The computations reported here are conducted with an in-house, unstructured grid code known as the General Equation and Mesh Solver (GEMS) code. [14, 15] The GEMS code solves the Navier-Stokes equations in conjunction with the continuity and energy equations described below. Laminar calculations were performed for all cases as there was interest in characterizing the laminar instability of the vena-contracta and that turbulence models for non-Newtonian fluids are not well developed. For a flow with a single species, a single momentum equation, a single energy equation, the Navier-Stokes equations that express the conservation principles are:

$$\frac{\partial Q}{\partial t} + \frac{\partial \left(E_i - E_{vi}\right)}{\partial x_i} = 0 \tag{1}$$

where the vectors, Q, E and E_{vi}, are given by

$$Q = \begin{pmatrix} \rho \\ \rho u_j \\ \rho h^0 - p \end{pmatrix} \tag{2a}$$

$$E = \begin{pmatrix} \rho u_i \\ \rho u_i u_j + \delta_{ij} p \\ \rho u_i h^0 - p \end{pmatrix} \tag{2b}$$

$$E_{vi} = \begin{pmatrix} 0 \\ \tau_{ij} \\ \tau_{ij} u_j + \lambda \frac{\partial T}{\partial x_i} \end{pmatrix} \tag{2c}$$

The quantities; x_i and u_i in Eqs. (1) and (2) represent the Cartesian coordinates and velocity components; p and ρ represent the pressure and density and h^0 is the stagnation enthalpy. τ_{ij} is the Reynolds stress tensor, λ is the thermal conductivity. A pseudo-time term expressed in terms of the primitive variables, $Q_p = (p, u_i, T)^T$, a pseudo time, τ, and a coefficient matrix, Γ, is added to the equation, so that the equation becomes:

$$\Gamma \frac{\partial Q_p}{\partial \tau} + \frac{\partial Q}{\partial t} + \frac{\partial (E_i - E_{vi})}{\partial x_i} = 0 \tag{3}$$

The matrix, Γ, is chosen to control the artificial dissipation in the spatial discretization and the convergence of the pseudo-time iteration.

The coefficient matrix, Γ, in the pseudo time term in Eq. (3) is defined by starting from the Jacobian of the conservative variables with respect to the primitive variables, $\partial Q/\partial Q_p$, and by replacing the physical property derivative, ρ_p, by an artificial property derivative, ρ'_p, as shown below:

$$\Gamma = \begin{pmatrix} \rho'_p & 0 & 0 & 0 & \rho_T \\ \rho'_p u & \rho & 0 & 0 & \rho_T u \\ \rho'_p v & 0 & \rho & 0 & \rho_T v \\ \rho'_p w & 0 & 0 & \rho & \rho_T w \\ \rho'_p h^0 - \left(1 - \rho h_p\right) & \rho u & \rho v & \rho w & \rho_T h^0 + \rho h_T \end{pmatrix} \tag{4}$$

The preconditioning method uses an artificial property derivative ρ'_p, which is dependent upon the local fluid dynamics scales. [16] This artificial term contributes to keeping the system well-conditioned for efficient solution and accurate formulation of the artificial dissipation terms. For the present calculations, ρ'_p is defined in term of Reynolds ($\mathrm{Re} = V \cdot \delta/\nu$),

$$\rho'_p = \frac{k_c}{V^2 \max\left(1, 1/(\mathrm{Re} \times AR)^2, 4\frac{\Delta p}{\rho}\right)} \tag{5}$$

where AR(>1) is the aspect ratio of the control volume that the conservation principle is applied. Δp is the pressure difference across the all the faces of a cell. [17] k_c is a constant chosen to ensure that $\rho'_p = \rho_p$ when the local velocity is equal to the physical speed of sound.

The flux formulation for a general upwind finite volume approach can be interpreted as the average of the fluxes on either side of the cell interfaces augmented by an artificial dissipation term,

$$\tilde{E} = \frac{1}{2}(E_L + E_R) - \frac{1}{2}|A|(Q_R - Q_L) = \frac{1}{2}(E_L + E_R) - \frac{1}{2}\Gamma\left|\Gamma^{-1}A_p\right|\left(Q_{pR} - Q_{pL}\right) \tag{6}$$

The acoustic eigenvalues, $\lambda_i^{\pm}$, of the matrix $\Gamma^{-1}A_p$, are given by

$$\lambda_i^{\pm} = \frac{1}{2}\left[u_n \cdot \left(1 + \left(\frac{c}{c'}\right)^2\right) \pm \sqrt{{u_n}^2 \cdot \left(1 - \left(\frac{c}{c'}\right)^2\right)^2 + 4c'^2}\right] \tag{7}$$

The quantity, c', in Eq. (7) is a pseudo speed of sound and u_n is the velocity component normal to the cell face. The pseudo speed of sound is calculated from:

$$c'^2 = \frac{\rho h_T}{\rho \rho'_p h_T + \rho_T\left(1 - \rho h_p\right)} \tag{8}$$

The numerical procedure uses a second-order approximate Riemann solver to evaluate the spatial fluxes at cell faces. Second-order temporal accuracy is achieved by means of an implicit dual time procedure that eliminates factorization errors.

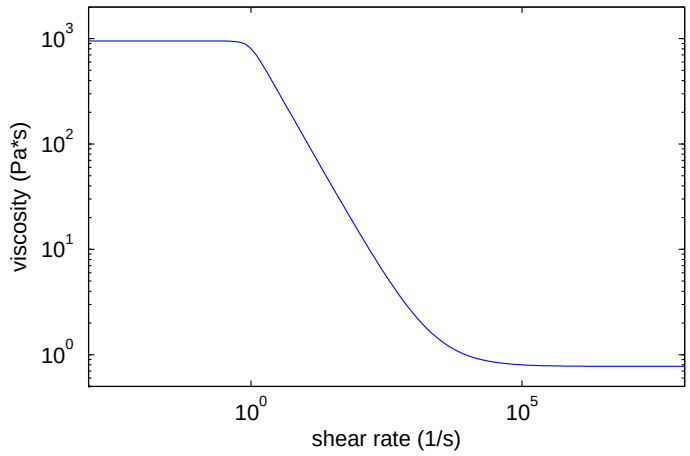

Figure 2: Viscosity curve of MMH/4% HPC Gel based on a C-Y model

2.2 Rheological Model

The rheological model is the most crucial to describe the realistic behaviour of the shear-thinning fluids. A Generalized Newtonian Constitutive (GNC) equation is widely used to define the non-linear relationship between the shear stress and deformation of the material. It remains a form of viscosity for Newtonian fluids by defining the viscosity as not a constant but a function of the shear rate as:

$$\tau_{ij} = -\eta(\dot{\gamma})\,\dot{\gamma}_{ij} \tag{9}$$

where, η is a viscosity function and $\dot{\gamma}_{ij}$ is the second-order strain rate tensor. The shear rate, $\dot{\gamma}$, is obtained by the second invariant of the strain rate as:

$$\dot{\gamma} = \sqrt{\frac{\prod_{\dot{\gamma}_{ij}}}{2}} = \sqrt{\frac{\dot{\gamma}_{ij} : \dot{\gamma}_{ij}}{2}} \tag{10}$$

The shear-thinning behavior is expressed by the viscosity function in Eq. (9). A variety of candidate models exist for the viscosity function. The viscosity curve of the shear-thinning fluids for gel propellant applications can be characterized from a series of rheological tests. Ciezki et al. [3] characterized the viscosity curve with plateaus for both low and high shear rate ranges and proposed the Herschel-Bulkley Extended model. The Carreau-Yasuda (C-Y) model adopted in the present study also contains the plateaus at both ends and additionally provides the smooth curve during the transitions, which is beneficial in numerical aspects in that a continuous viscosity function is prescribed over the entire shear rate space. The C-Y model is expressed as:

$$\frac{\eta(\dot{\gamma}) - \eta_\infty}{\eta_0 - \eta_\infty} = \left[1 + (\dot{\gamma}\lambda)^a\right]^{\frac{n-1}{a}} \tag{11}$$

where, a, n, and λ are the fitting coefficients; η_0 and η_∞ is the viscosity plateau at ultimate low and high shear rate, respectively. Our computations are conducted using the rheological properties of MMH/HPC gel that exhibits the pure shear-thinning behavior by previous experiments [19] and have been used as a gelled fuel. The viscosity curve of MMH/HPC gel is represented in Figure 2 by C-Y coefficients: $\eta_0 = 950Pa*s^n$, $\eta_\infty = 775mPa*s^n$, $\lambda = 1.07$, $a = 4.76$, and $n = 0.09$. Also, note that the density of the fluid in the present study is assumed as 870 kg/m^3 for MMH/HPC gel.

2.3 Computational Mesh and Boundary Condition Treatments

The computational mesh in the present study consists of a hemisphere (injector manifold) and cylinder (orifice) as depicted in Figure 3 for a upstream manifold and orifice tube, respectively. The interface between the hemisphere and cylinder is smoothly rounded with a small radius, r/D = 0.05, to avoid singularities. The grid points are stretched in a direction away from wall surfaces and the hemisphere/cylinder interface. Butterfly meshing is used in the cylinder is utilized for efficient cell arrangements inside a boundary layer. The density of the computational mesh is preserved even under different orifice lengths in a further parametric study.

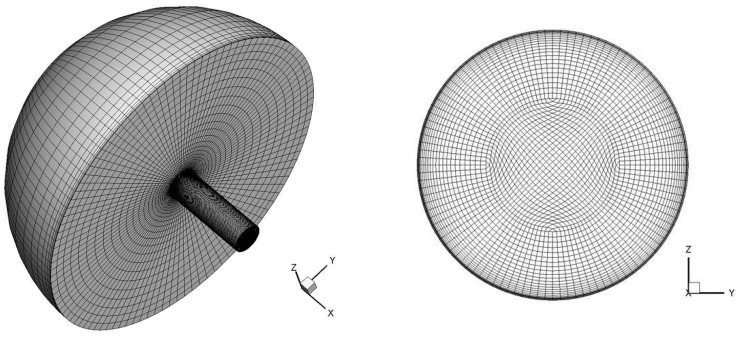

(a) Front view (b) Orifice Cross-section

Figure 3: Computational meshes

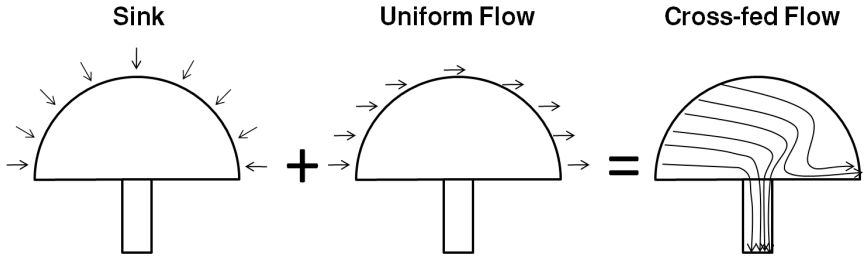

Figure 4: Upstream Boundary Condition Treatments for Cross-Fed Orifice Flows using a Potential Flow Theory

Using computational meshes above, a potential flow theory is utilized to obtain inflow conditions on the hemispherical injector manifold boundary as illustrated in Figure 4. A sink located at the center of orifice inlet is superposed with a uniform manifold cross-flow velocity to derive the pertinent velocity components on the hemispherical boundary. This method excludes the cyclone effect that may be present with other orifices in close proximity. The resulting velocity components on the hemispherical boundary may be expressed:

$$u = \frac{Q}{2\pi R^2} \sin\theta \sin\phi \tag{12a}$$

$$v = \frac{Q}{2\pi R^2} \cos\theta + V_1 \tag{12b}$$

$$w = \frac{Q}{2\pi R^2} \sin\theta \cos\phi \tag{12c}$$

where Q is a volumetric mass flow rate, R is a radius of a hemisphere, $\theta = \cos^{-1}(y/R)$, and $\phi = \sin^{-1}(x/R\sin\theta)$.

In addition to the upstream boundary condition, a constant back pressure is imposed at the downstream boundary and the rest of boundary planes are treated as a no-slip wall. While it would be desirable to extend the computational domain into the downstream chamber (at considerable expense), prior simulations [13] indicate a good capabiity to predict mean and bulk transient oscillation modes with the selected domain. During the computation, the upstream pressure is controlled by specified inflow velocity components and gradually reaches a quasi-equilibrium state as a quasi-periodic flow evolves in the injector passage.

2.4 Convergence Study

A grid convergence study was conducted to determine the mesh size for a parametric study in the following sections. According to the results of the convergence study in previous axisymmetric calculations [9], 160 * 72 grid points (axial and radial grid number, respectively) are chosen for the surface mesh to be revolved for full three-dimensional mesh. Thus, four candidate grids were prepared with respect to the azimuthal grid number in the convergence study. The unsteadiness is quantified by the mean discharge coefficient (C_D), oscillation amplitude of C_D, and Strouhal number,

Table 1: Summary of a convergence study

Label	Azimuthal Grid #	Total Cell #	C_D	$3\sigma(C_D)$ (%)	St
Grid A	36	149,720	0.60	1.46	0.43
Grid B	72	324,860	0.65	3.39	0.29
Grid C	**108**	**529,160**	**0.65**	**3.66**	**0.54**
Grid D	144	762,620	0.64	3.79	0.51

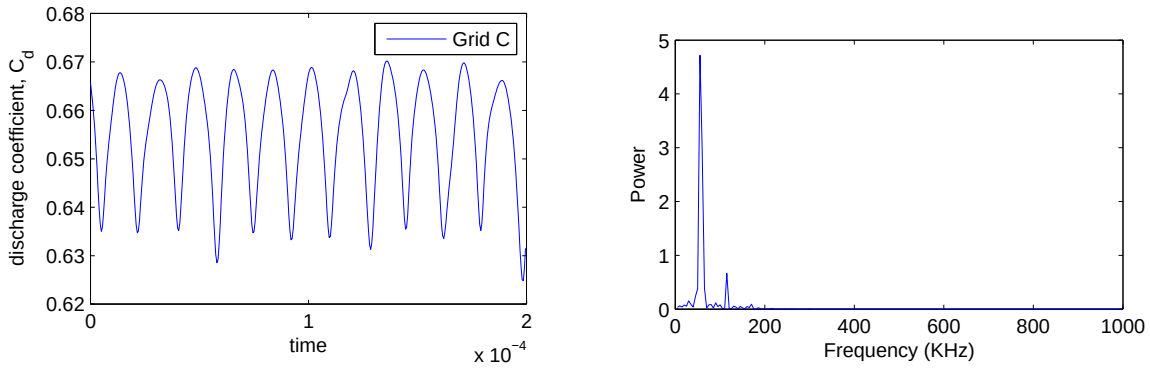

(a) Mass pulsation history

(b) FFT analysis of a pulsation

Figure 5: Unsteady solution of Grid C for Baseline case ($Re_\infty = 15,700$, $Re_{gen} = 1,200$, sharp-edged orifice inlet, and L/D = 3 with a MMH/HPC gel)

St. In particular, the oscillation amplitude is obtained by a statistical quantity as $3\sigma(C_D)$ to exclude the irregular peaks during the unsteadiness mode. In addition, the discharge coefficients in the present study need to include the cross velocity in a manifold. The discharge coefficient and Strouhal number are defined as:

$$C_D = \frac{\dot{m}}{\rho V_B A} = \frac{V_2}{\sqrt{\frac{2\Delta p}{\rho} + V_1^2}} \tag{13a}$$

$$St = fV_2/D \tag{13b}$$

Where V_1 and V_2 is a cross and ideal (Bernoulli) orifice exit velocity, respectively, f is the oscillation frequency, and D the orifice diameter.

For a baseline case, $V_1/V_2 = 0.3$, $V_2 = 27.5m/s$ and sharp-edged (r/D = 0.05) L/D = 3.0 orifice geometry in which the unsteadiness is estimated to arise was chosen to characterize the natural oscillation during the unsteadiness. As a result, periodical oscillations are observed as Figure 5(a). These hydrodynamics instabilities inside an orifice passage are characterized using a Fast Fourier Transformation (FFT) as shown in Figure 5(b). The data sampling is initiated after the solutions adequately reach a quasi-periodic state as shown in Fig. 5(a) and pressure oscillations at the inlet boundary are less than 1%.

This baseline case is used to determine the effective grid size for the following parametric investigation. Four different grids are used for the convergence tests. Their grid densities are controlled by grid points in an azimuthal direction. As the total cell number increases from Grid A to Grid D, the mean discharge coefficient, C_D, converges to a value of 0.65, and oscillation amplitude increases. The Strouhal number reaches a value of 0.54, which is quite close to the value obtained for the densest mesh of 0.51. Therefore, Grid C is chosen as a grid for a parametric study as a practical level given the desire to conduct parametric studies. Users should be aware that computational uncertainty in the unsteady characteristics is fair but not excellent under the meshes employed.

3. Analysis of Hydrodynamic Instabilities

The typical structure of cross-fed orifice flows for both Newtonian and shear-thinning fluids is represented in Figure 6. Some fraction of the stream tube containing the cross-flowing manifold flow is captured by the orifice itself. While

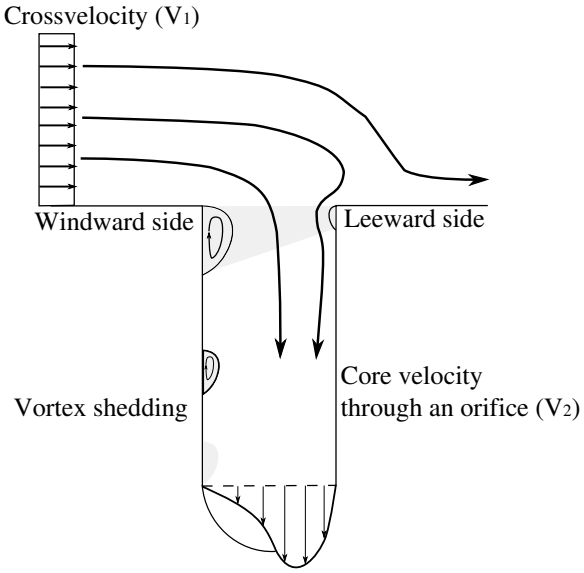

Figure 6: Typical flow structure of cross-fed orifice flows

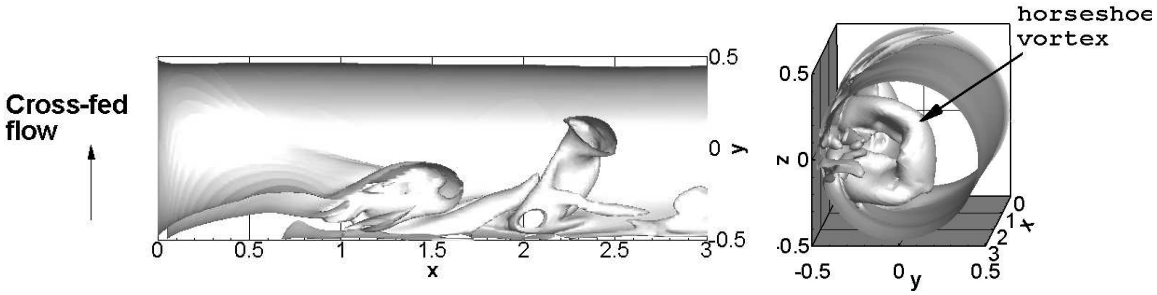

(a) Cross-sectional view (b) Downstream view

Figure 7: Vortex generation of a cross-fed orifice flow for a shear-thinning fluid (an iso-surface of the vorticity magnitude = 50,000)

the fluid accelerates into the orifice, an asymmetric vena-contracta is formed at the inlet lip. Vortices shed in the axial direction from the windward side of the vena-contracta are larger in extent than those shed from the leeward side. Depending on the cross-flow/axial flow velocity ratio, the vena-contracta and axially-shed vortices may be absent altogether on the leeward side of the passage. The axially-traveling vortex structure is connected smoothly azimuthally, thereby forming a three-dimensional ring vortex ring that has a variable thickness.

The flowfield in question is fairly analogous to flow in a curved pipe flows in that twin eddies arise in the orifice due to the azimuthal pressure gradient emanating from the leeward surface. As the fluid moves along the orifice passage, the twin eddy structure is violently deformed and collapsed by the vortex ring in a vena contracta. Furthermore, the vortex ring is naturally unstable, oscillates, and distorts in the stream-wise direction. Finally, this unsteady motion gives way to the vortex separation and shedding, and eventual decay or breakdown to the fine scale structure if the orifice tube is sufficiently long. In general, the passage lengths of interest do not permit full decay and definite memory of the asymmetric inlet flow is present at the orifice exit. These processes induce periodic formation and shedding of horseshoe vortices generation as shown in Figure 7.

Figures 8 and 9 assess effects of crossflow and fluid rheology on vorticity evolution in the orifice passage. Both calculations retain the same orifice design and mean massflow as in Fig. 7. In Fig. 8, a fully 3-D calculation is performed on an axially-fed passage (i.e. zero crossflow) using the shear thinning fluid rheology described in Fig. 2. The result shows vorticity confined to a narrow region near the periphery of the channel in good agreement with prior axisymmetric calculations [9]. The vortex ring at the vena contracta is formed with a constant thickness in the azimuthal direction. The flowfield is still unsteady as satellite vortices are separated from the main vortex ring and

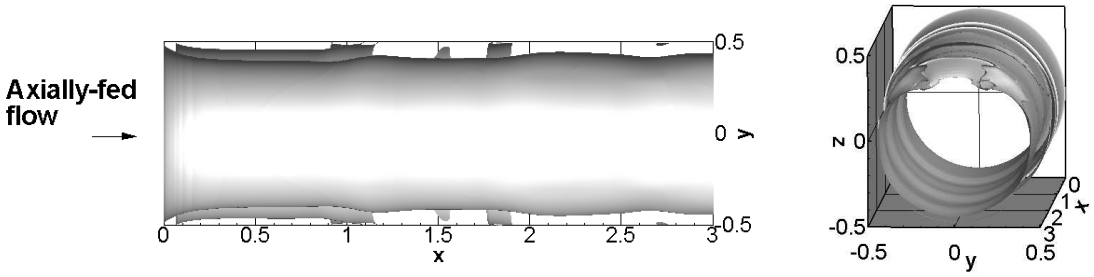

(a) Cross-sectional view (b) Downstream view

Figure 8: Vortex generation of a axially-fed orifice flow for a shear-thinning fluid (an iso-surface of the vorticity magnitude = 50,000)

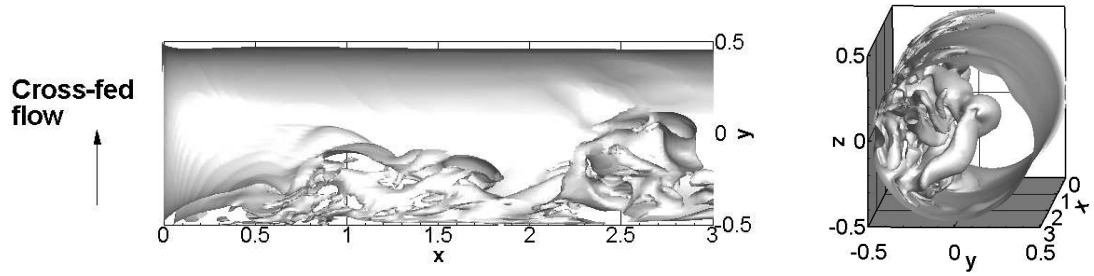

(a) Cross-sectional view (b) Downstream view

Figure 9: Vortex generation of a cross-fed orifice flow for a Newtonian fluid (an iso-surface of the vorticity magnitude = 50,000)

convect downstream. This process leads to a wrinkled vorticity iso-surface at any given instant in time as noted in Fig. 8.

Figure 9 highlights the influence of fluid rheology and compares a Newtonian liquid with the shear-thinning result in Fig. 7. Water, with viscosity and density of 0.001 Pa*s, and 1000 kg/m^3 is used for the calculation. As shown in Figure 9, the vorticity structure is more complicated and finer than for shear-thinning fluid simulation in Fig. 7. The Newtonian result still shows the evolution of the horse shoe vortex encompassing a substantial fraction of the span of the channel, but it is perhaps not as distinct as in shear-thinning result. Note that this laminar simulation has a limitation in describing the fine-scale turbulence motion that is created by the vortex breakdown and can only be used to interpret the major vortical structures in the flowfield.

For shear-thinning fluids, the unsteadiness creates both massflow and viscosity fluctuations. When the cross velocity in the manifold is non-zero, spatial asymmetry of the axial velocity, Figure 10(a), and viscosity, Figure 10(b), is enlarged in the transverse direction. The expansion of the vena-contracta on the windward side cause the strong acceleration of the fluid on the opposite side and travelling vortices create axial velocity/mass pulsations. The unstable motion of the vena-contracta can be understood as an oscillating behaviour of the shear layer. For the shear-thinning fluids, the shear layer is closely related with the viscosity because of the shear rate dependence. Subsequently, the lowest viscosity region attached to the inlet corner oscillates up and down in a transverse direction. The high viscosity zone is significantly influenced by this oscillation and passes through the exit hole periodically as seen Figure 10(b).

Hydrodynamic instabilities are known to contribute to atomizing the emerging jets by creating and enhancing disturbances on the free surface near the exit of the orifice. These intensified disturbances trigger instabilities in the free surface ultimately affecting the size of ligaments and droplets shed from this surface[20]. Evolution of the spray pattern imposed by assymetry from a relatively short orifice with cross-flow has not been studied in the literature even though there are obvious differences in the character of the massflux leaving the orifice in this case.

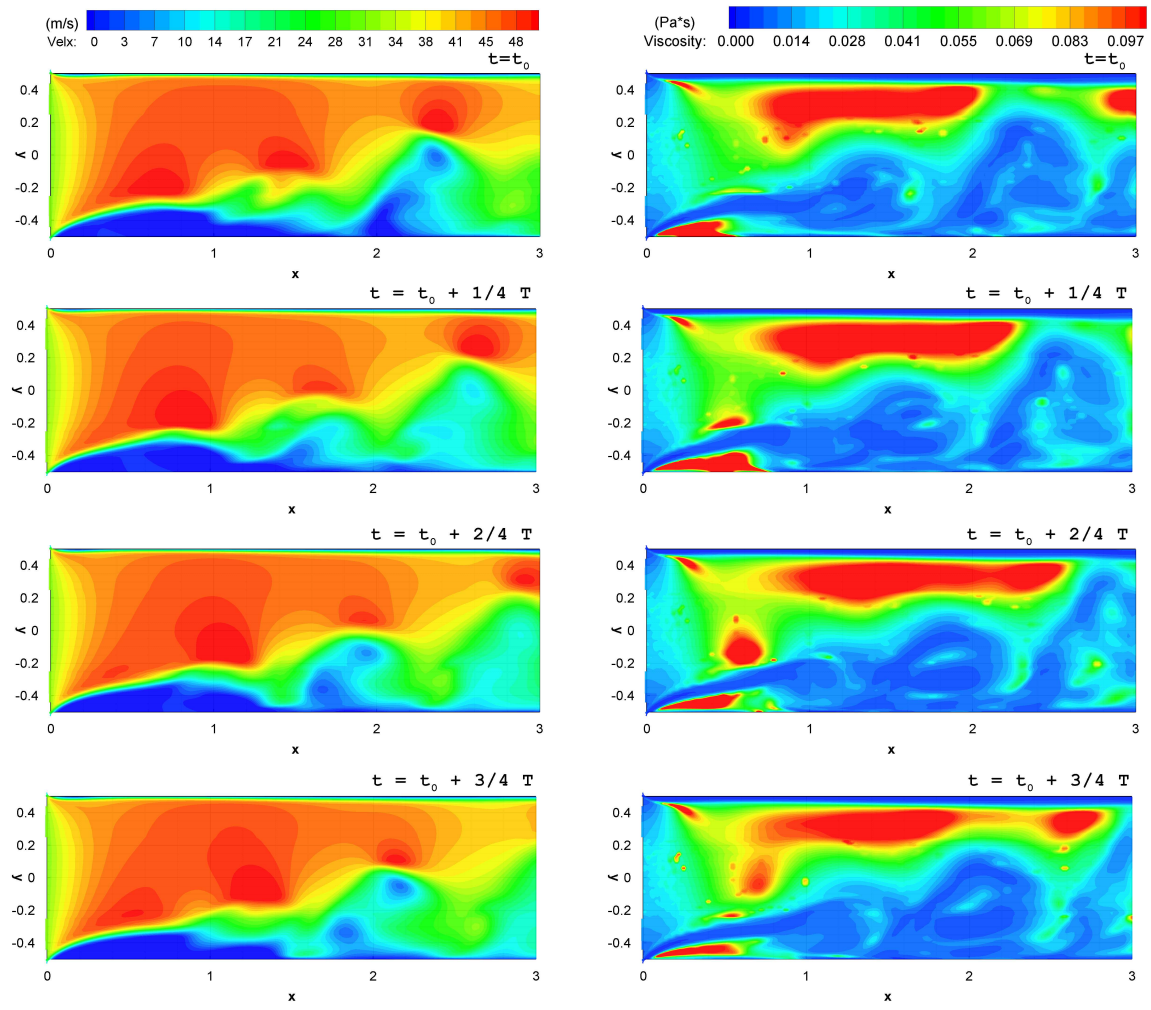

(a) Axial velocity contour

(b) Viscosity contour

Figure 10: Instantaneous axial velocity and viscosity contours at various times in a quasi-periodic oscillation.

Table 2: Cases Investigated

L/D	V_1/V_2	Re_∞	Re_{gen}
3, 4, 5, 6	**0.30**	**15700**	**1200**
3	0, 0.15, 0.30, 0.44, 0.58	15700	1200
3	0.30	3900, 7800, 11700, 15700, 19600, 23500	100, 360, 730, 1200, 1720, 2300

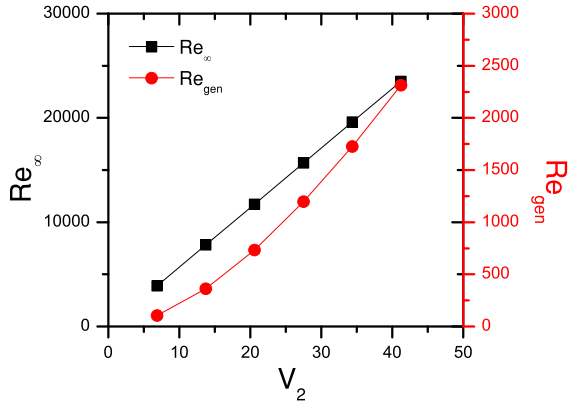

Figure 11: Reynolds numbers with respect to core velocity V_2

4. Parametric Studies

The effects of the orifice length-to-diameter (L/D) ratio, cross-to-core velocity ratio (V_1/V_2), and Reynolds number were assessed in a series of parametric studies. A total of 13 simulations were conducted in support of these parametrics as indicated in Table 2. The baseline conditions, employed in the grid convergence study and in results in Figs. 5, 7, and 10, are highlighted in bold in Table 2. The orifice L/D ratios were controlled by changing orifice length given a constant orifice diameter. A very short orifice length is known to cause hydraulic flip at a high speed injection condition, and the range of L/D ratio in the present study is limited from 3 to 6. In addition, the velocity ratio is varied by a magnitude of the cross velocity in a manifold up to $V_1/V_2 = 0.3$ fixing the core velocity, V_2, through an orifice. The Reynolds numbers of such flows are determined by the flow speed of the interest which reflects the practical injection operation range. In this respect, the Reynolds number is obtained by its own definition equivalent to the bulk injection velocity, V_2 = 10 - 60 m/s. For non-Newtonian fluids, the generalized Reynolds number is used to reflect the variable viscosity. Its definition depends on the chosen model in order to describe the viscosity curve. For C-Y model, the generalized Reynolds number can be expressed as [9]:

$$\mathrm{Re}_{gen} = \frac{\rho V_2}{\left[\left[1+\left\{\lambda\left(\frac{3n+1}{4n}\right)\frac{8V_2}{D}\right\}^a\right]^{\frac{n-1}{a}}(\eta_0-\eta_\infty)+\eta_\infty\right]\left(\frac{3n+1}{4nD}\right)} \tag{14}$$

$$\mathrm{Re}_\infty = \frac{\rho V_2 D}{\eta_\infty} \tag{15}$$

However, considering that hydraulic instabilities near the inlet lip occur with a minimum viscosity near the high shear rate Newtonian plateau, the Reynolds number based on η_∞, Eq. (14), can also be useful to characterize the instabilities. Consequently, the Reynolds number based on η_∞ is also included in the flow characterization. Figure 11 provides a comparison of the two Reynolds numbers for the range of injection velocities considered in the parametric studies.

4.1 Effects of Orifice Length-to-Diameter Ratios

The discharge coefficients for shear-thinning fluids are presented with one for Newtonian fluids in Figure 12. The data for Newtonian fluids are obtained from Nurick et al.'s experimental correlations. The discharge coefficients for

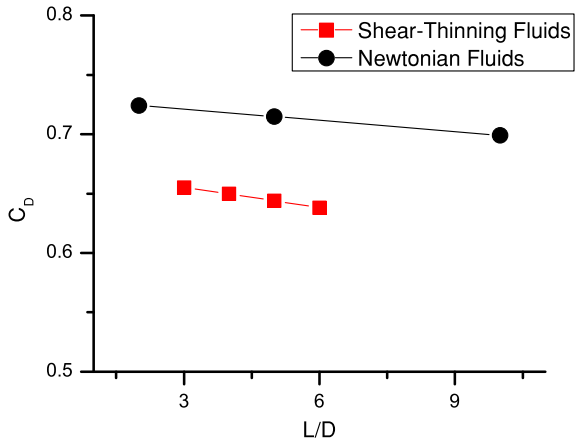

Figure 12: Discharge coefficients in terms of orifice L/D ratio

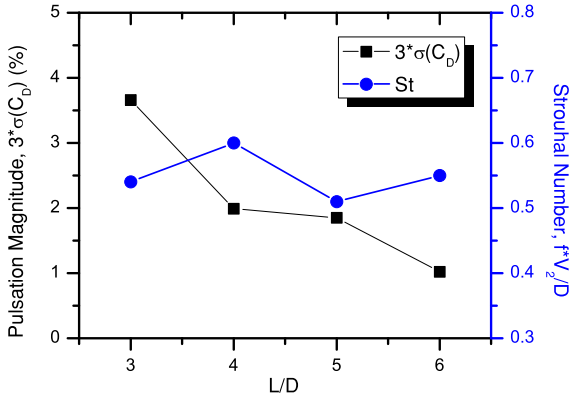

Figure 13: Pulsation magnitude and Strouhal number in terms of orifice L/D ratio

shear-thinning fluids are about 10% lower than ones for Newtonian fluids and tend to degrade more rapidly with L/D increases than the Newtonian counterparts. Viscous drag against the walls of the orifice is of course more prominent with the gelled fluids and for this reason lower L/D passages will be desired for injectors designed with these higher viscosity fluids.

The unsteady characteristics of the simulations in Fig. 12 are presented in Fig. 13. Substantial unsteadiness is present in the flow as massflow pulsations as large as nearly 4% occur. This pulsation level is substantially greater than that computed for axisymmetric flows[9]; one might expect that this could have profound effects on atomization character and spray evolution as a result. As the orifice L/D ratio increases, the separated vortex decays to a greater extent during its transit through the orifice passage, and the pulsation strength is correspondingly diminished. The Strouhal numbers characterizing the fundamental frequency of the pulsations, range from 0.5 to 0.6 and do not change a lot under the limited range of L/D ratios investigated. These values are substantially larger than the 0.2-0.3 range found for axisymmetric (i.e. no crossflow) inlet conditions[9]. At this special velocity ratio it appears that the subharmonic tone is nearly as powerfull as the primary harmonic as discussed in the study of crossflow velocity in the following subsection.

4.2 Effects of Manifold Crossflow Velocity

The discharge coefficients from the present simulations are represented with ones from Nurick's experimental correlations [12] at the orifice L/D = 2 and 5 in Figure 14. Here, the velocity ratio V_1/V_2 is controlled by the change of the cross velocity V_1 in a manifold fixing the injection velocity V_2. As V_1 increases, the discharge coefficient decreases for both fluids. For shear-thinning fluids, the discharge coefficient is much more sensitive to crossflow, and at $V_1/V_2 = 0.6$,

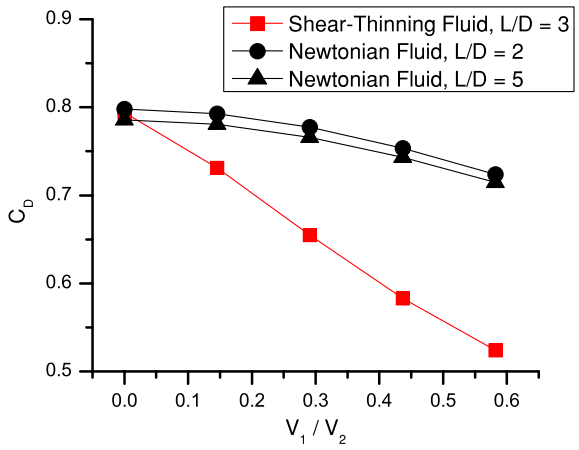

Figure 14: Discharge coefficients in terms of V_1/V_2

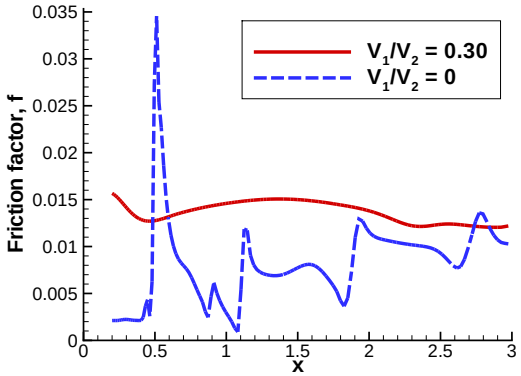

Figure 15: Distribution of the time-averaged local friction factor on the leeward side at Z = 0

it reaches to about 30% lower value than straightly-fed case ($V_1/V_2 = 0$). This implies that under a given pressure drop condition, the actual mass flow rate for shear-thinning fluids can be strongly influenced by the velocity ratio and that careful manifold designs will be required for multi-element injectors using gelled fluids. This significant reduction of discharge coefficients seem to be caused by the unusually strong and unbalanced flow resistance on the leeward side of the passage as Figure 15.

The effect of V_1/V_2 ratio on oscillation characteristics are shown in Figure 16. As the velocity ratio increases the pulsation magnitude increase. Typical values determined in prior axisymmetric (i.e. axially-fed) simulations were of the order of 1-2%; crossflow is tending to increase pulsation magnatudes by factor of 3-5 times. The enhanced size of vena-contracta and the transverse transport of vorticity leads to the increase in the pulsation levels under crossflow conditions. We anticipate larger fluctuations in the crossflow-fed spray as a result. Unfortunately, this is typically difficult to observe as most examples of crossflow-fed orifices occur in multi-element configurations in which individual orifice contributions are difficult to ascertain. A focused study in this area would be of great interest.

In spite of the change of pulsation magnitude, the Strouhal number is almost constantly remained except for $V_1/V_2 = 0.3$ case. For all cases, one cycle of discharge coefficient contains two peaks: a strong and weak peak. At $V_1/V_2 = 0.3$, two peaks are almost similar in a magnitude as Figure 5(a), and one dominant frequency, two times of the previous frequency, is detected. At this special velocity ratio, the subharmonic is virtually as powerful as the prime harmonic tone. This is supported by the FFT analysis which provides two dominant Strouhal numbers: 0.54 and 0.27.

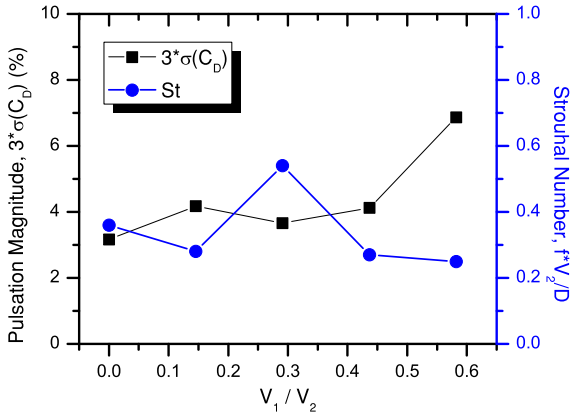

Figure 16: Pulsation magnitude and Strouhal number in terms of V_1/V_2

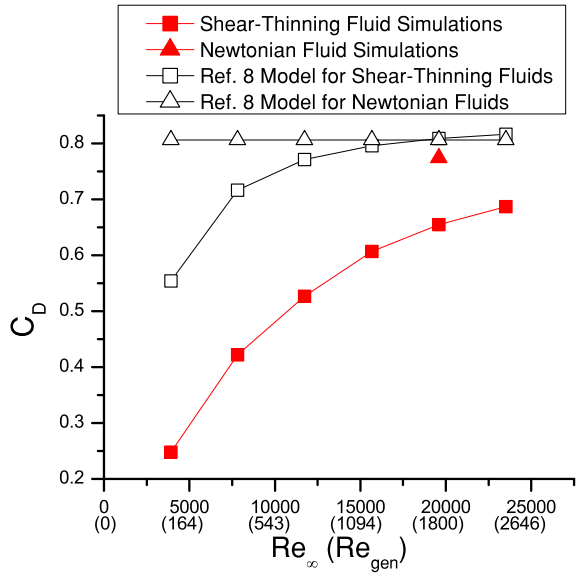

Figure 17: Discharge coefficient in terms of Reynolds number

4.3 Effects of Reynolds Numbers

Fixing $V_1/V_2 = 0.3$ and orifice L/D = 3, the Reynolds number is varied by the change of the core velocity V_2. Here, the Reynolds number based on η_∞ is considered to compare with the flow characteristics for Newtonian fluid simulation and data from other literature. The discharge coefficients are compared with one from Newtonian fluid simulation and solutions from a potential flow theory for cross-fed orifice flow by Strakey and Talley [10] in Figure 17. As expected, the discharge coefficients for shear-thinning fluids are overall lower than those for Newtonian fluids. The shear-thinning fluids are more sensitive to Reynolds number due to the fact that generalized values that reflect some of the viscous character are substantially lower than the values based on the Newtonian limit viscosity. For Newtonian cross-fed orifice flows, Ref. [10] model is known to exhibits the good accuracy in a prediction of discharge coefficient and this point is again confirmed by a simulation result and its prediction from a potential flow theory at $Re_\infty = 20,000$. However, Ref. [10] model fails to a prediction of discharge coefficient for shear-thinning fluids even though the friction factor is corrected for shear-thinning fluids. The effect may be attributed to the overestimation of the vena-contracta size in shear-thinning fluids in a potential flow model. The potential flow model provides the contraction coefficient, 0.607, at $V_1/V_2 = 0.3$, but the actual simulation exhibits the vena contracta much smaller than a half of the cross-sectional area, which implies that the contraction coefficient is less than 0.5.

The oscillation characteristics as a function of Reynolds number are summarized in Figure 18. For $Re_\infty <$

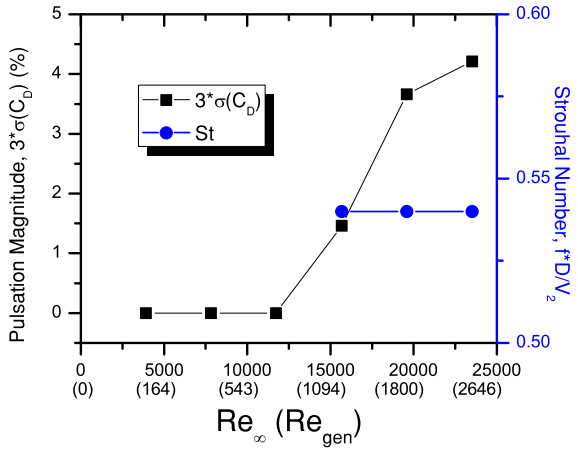

Figure 18: Pulsation magnitude and Strouhal number in terms of Reynolds number

15, 000, a steady flow is obtained with the shear thinning fluid. At higher Reynolds numbers, unsteady flows appear and the Strouhal number is constant over the remaining range investigated. When the hydrodynamic instabilities are present, the oscillation frequency proportionally increases with increasing flow speed V_2. Similar behavior was noted for Newtonian fluids by Bunnell and Heister[13].

5. Summary and Conclusions

The present study is aimed to reveal the flow structure of cross-fed orifice flows and to characterize them in terms of orifice length-to-diameter ratio, cross velocity in a manifold, and Reynolds number. The numerical model considered in the present study is based on a full laminar Navier-Stokes equation solver including a rheological modeling. The boundary condition is treated by a potential flow theory in order to describe the cross-fed flows in a manifold.

Compared with straightly-fed and Newtonian flow simulation, cross-fed orifice flows for shear-thinning fluids have larger and more distinct vortex structure generated by the horseshoe vortex than for Newtonian fluids and are observed to have quite spatially biased unsteadiness. Also, according to a parametric study, the conclusions that can be drawn are as followings.

1. The discharge coefficients decreases as the orifice L/D ratio increases and the Strouhal number ranges from 0.5 to 0.6.

2. As the cross velocity increases, the discharge coefficients are significantly reduced due to its strong and unbalanced flow resistance due to a shear thinning behavior. A period of oscillations are found to have two peaks, a strong and weak peak, over the investigated V_1/V_2 range, $0 < V_1/V_2 < 0.6$, except for 0.3. At $V_1/V_2 = 0.3$, a strength of the weak peak during a period grows, and finally Strouhal number becomes 0.54, a double of Strouhal number under other V_1/V_2s.

3. The previous analytical model for discharge coefficients [10] that agrees well to a Newtonian orifice flows fails to the prediction of shear-thinning orifice flows. It is guessed by the overprediction of a size of vena contracta. At Re_∞<25,000, the discharge coefficient largely increases as Reynolds number increases. It is also found that the Reynolds number is independent on oscillation behaviors.

Acknowledgments

The authors acknowledge the support of the Army Research Office and Program Manager Dr. Ralph Anthenien in sponsoring the subject work under the Multi-University Research Initiative (MURI) grant number W911NF-08-1-0171.

References

[1] Hodge, K., Crofoot, T., and Nelson, S. 1999. Gelled Propellants for Tactical Missile Applications. In: *35th AIAA/ASME/SAE Joint Propulsion Conference*. AIAA paper 99–2976.

[2] Rahimi, S., Hasan, D., and Peretz, A. 2004. Development of Laboratory-Scale Gel-Propulsion Technology. *Journal of Propulsion and Power*, 20:93–100.

[3] Kampen, J. V., Alberio, F., and Ciezki, H. K. 2007. Spray and Combustion Characteristics of Aluminized Gelled Fuels with an Impinging Jet Injector. *Aerospace Science and Technology*, 11:77–83.

[4] Rahimi, S. and Natan, B. 2000. Flow of Gel Fuels in Tapered Injectors. *Journal of Propulsion and Power*. 16:458–464.

[5] Natan, B. and Rahimi, S. 2000. Numerical Solution of the Flow of Power-Law Gel Propellants in Converging Injectors. *Propellants, Explosives, Pyrotechnics*, 25:203–212.

[6] Lichtarowicz, A., Duggins, R. K. and Markland, E. 1976. Discharge Coefficients for Incompressible Non-Cavitating Flow Through Long Orifices. *Journal of Mechanical Engineering Science*, 7:210–219.

[7] Canino, J. and Heister, S. D. 2009. Contributions of Orifice Hydrodynamic Instabilities to Primary Atomization. *Atomization and Sprays*. 19:91–102.

[8] MacDonald, M., Canino, J. and Heister, S. D. 2007. Nonlinear Response of Plain-Orifice Injectors to Nonacoustic Pressure Oscillations. *Journal of Propulsion and Power*. 23:1204–1213.

[9] Yoon, C., Heister, S., Xia, G., and Merkle, C., 2011. Numerical Modeling of Injection of Shear-Thinning Gel Propellants through Plain-Orifice Atomizer. *Journal of Propulsion and Power* (accepted).

[10] Strakey, P. A. and Talley, D. G. 1999. The Effect of Manifold Cross-Flow On The Discharge Coefficient Of Sharp-Edged Orifices. *Atomization and Sprays*. 9:51–68.

[11] Nurick, W. H., Ohanian, T., Talley, D. G. and Strakey, P. A. 2008. Impact of Manifold-to-Orifice Turning Angle on Sharp-Edge Orifice Flow Characteristics in Both Cavitation and Noncavitation Turbulent Flow Regimes. *Journal of Fluids Engineering*, 130:121102-1–121102-10

[12] Nurick, W. H., Ohanian, T., Talley, D. G. and Strakey, P. A. 2009. Impact of Orifice Length/Diameter Ratio on 90 deg Sharp-Edge Orifice Flow With Manifold Passage Cross Flow. *Journal of Fluids Engineering*. 131:081103-1–081103-10.

[13] Bunnell, R. A. and Heister, S. D. 2000. Three-Dimensional Unsteady Simulation of Cavitating Flows in Injector Passages. *Journal of Fluids Engineering*. 122:791–797.

[14] Li, D., Sankaran, V. and Merkle C. L. 2004. Computational Framework for Complex Fluids Applications. In: *3rd International Conference on Computational Fluid Dynamics*. 619–624.

[15] Xia, G., Sankaran, V., Li, D., and Merkle C. L. 2006. Modeling of Turbulent Mixing Layer Dynamics in Ultra-High Pressure Flows. In: *36th AIAA Fluid Dynamics Conference and Exhibit*. AIAA paper 2006–3729.

[16] Choi, Y. H. and Merkle, C. L. 1993. The Application of Preconditioning in Viscous Flows *Journal of Computational Physics*. 105:207–223.

[17] Darmofal, D. L. and Siu, K. 1997. A Robust, Multigrid Algorithm for the Euler Equations with Local Preconditioning and Semi-Coarsening. *Journal of Computational Physics*, 151:728–756.

[18] Ganippa, L. C., Bark, G., Andesson, S., and Chomiak, J. 2004. Cavitation:a contributary factor in the transition from symmetric to asymmetric jets in cross-flow nozzles. *Experiments in Fluids*, 36:627–634.

[19] Arnold, R., Santos, P. H. S., deRidder, M., Campanella, O. H., and Anderson, W. E. 2010. In: *48th AIAA Aerospace Science Meeting*. AIAA paper 2010–422.

[20] Heister, S. D., "Plain Orifice Spray Nozzles", Ch. 27, *Handbook of Atomization and Sprays, N. Ashgriz, editor*, Springer Publishers, New York, 2011.